International Journal of Coal Geology 146 (2015) 68–78

Contents lists available at ScienceDirect

International Journal of Coal Geology

journal homepage: www.elsevier.com/locate/ijcoalgeo

A preliminary study on the characterization and controlling factors of porosity and pore structure of the Permian shales in Lower Yangtze region, Eastern China

Lei Pan [a,b], Xianming Xiao [a,*], Hui Tian [a], Qin Zhou [a], Ji Chen [a,b], Tengfei Li [a,b], Qiang Wei [a,b]

[a] State Key Laboratory of Organic Geochemistry, Guangzhou Institute of Geochemistry, Chinese Academy of Sciences, Guangzhou 510640, China
[b] University of Chinese Academy of Sciences, Beijing 100049, China

ARTICLE INFO

Article history:
Received 11 September 2014
Received in revised form 2 May 2015
Accepted 12 May 2015
Available online 16 May 2015

Keywords:
Adsorption isotherm
BET
Porosity
TOC
Permian shale
Lower Yangtze region

ABSTRACT

Permian organic-rich shales occur throughout the Lower Yangtze region in Eastern China and are potentially a future target for shale gas exploration. Due to the lack of data, the gas potential of these Permian shales is difficult to evaluate. In this study, a total of 22 Permian shale samples were collected from two wells and their geochemical and rock property (porosity) characteristics were investigated. The results show that the samples have a total organic carbon (TOC) content of 0.6–17.4 wt.% derived from mainly gas-prone kerogen with a vitrinite reflectance (R_o) value ranging from 2.3 to 2.7%. Total porosity of the samples ranges between 1 and 5.5%. The micropore and mesopore surface areas range between 5.41–35.69 m^2/g and 3.59–11.23 m^2/g, respectively. Micropore and mesopore volumes range between 0.22–1.44 $cm^3/100$ g and 0.67–1.76 $cm^3/100$ g, respectively. Total porosity and pore structure data of these samples show a correlation with TOC. For samples with TOC < 12 wt.%, their total porosity has a positive correlation with TOC, while for samples with TOC > 12 wt.%, negative correlation relationships were observed. TOC content strongly impacts gas storage capacity of the Permian shales in the Lower Yangtze region, and the preliminary results of the present study have important implications for the shale gas play evaluation in this area.

1. Introduction

Paleozoic shales are distributed extensively in Southern China and have attracted much attention for shale gas exploration. Of these, the marine deposits of the Lower Cambrian and Lower Silurian in and around the Sichuan Basin were the focus of investigations in recent years (Hao and Zou, 2013; Huang et al., 2012a,b; Tian et al., 2013; Wang et al., 2009; Zhang et al., 2008, 2011; Zou et al., 2010) and as a result, commercial shale gas production is taking place in one block of the Fuling area (Guo and Zhang, 2014; MLRC, 2014; Zou et al., 2010).

The interest in these Permian shales in this area as economic shale gas exploration and development targets is particularly high due to the large regional extent, shallow burial (generally 2000–4000 m compared to 4000–6000 m deep burial of the Lower Paleozoic shales) allies their organic richness and their large thickness (100–600 m) (Guo et al., 1998; Ma et al., 2004; Pan et al., 2011; Wu et al., 2013; Xu, 2013; D.W. Zhang et al., 2012; Zhou et al., 2012). According to the study by D.W. Zhang et al. (2012), the gas resources of the Permian shales in the Lower Yangtze region are estimated to be 1.55×10^{12} m^3 (~54 tcf) and thus represent an enormous potential for hydrocarbon exploration and development.

The shales were deposited in a marine–terrestrial transitional environment (Ding et al., 1987; Liang et al., 2009) and are mostly gas-prone in contrast to the oil-prone marine shales of the Lower Paleozoic (Chen et al., 2013; Liang et al., 2009; Xu et al., 2011). The thermal maturity of the Permian shales varies, but is mostly in the dry gas window with vitrinite reflectance (R_o) of 1.5–2.5% (Pan et al., 2011; Wu et al., 2013) and up to >3% where greater heat flow (magmatic influence) is present (Ma et al., 2004; Wu et al., 2002). Previous studies on the shales mainly focused on sequence stratigraphy, paleodepositional environment and conventional hydrocarbon potentials (Du et al., 1999, 2010; Wu and Li, 2001) with little interest in the unconventional resource evaluation. Recently, two exploration wells have been drilled in the Wuhu County to assess the thick organic-rich Permian shales. Core samples collected from the two wells were investigated for porosity and pore structure and compared with geochemical data in order to evaluate some possible controlling factors. The data are presented and discussed here in the context of the gas potentials of these unconventional shale reservoirs.

2. Geological setting

The Lower Yangtze region covers an area of about 22.5×10^4 km^2. It is bounded by the East China Sea and the Yellow Sea to the east and northeast, by the Tanlu Fault to the west and northwest, and by the

* Corresponding author. Tel.: +86 2085290161; fax: +86 2085290706.
E-mail address: xmxiao@gig.ac.cn (X. Xiao).

http://dx.doi.org/10.1016/j.coal.2015.05.005
0166-5162/

Jiangnan Uplift and Huaxia Uplift to the south and southeast (Guo et al., 1998; Pan et al., 2011; Fig. 1). The sedimentary–tectonic evolution of the Lower Yangtze region encountered three main stages (Yuan et al., 2006): marine sediment deposition from Early Paleozoic to Middle Triassic, terrestrial sediment deposition from Late Triassic to Early Cretaceous (Fig. 2), and burial and tectonic deformation and overprint through the Late Cretaceous to Cenozoic. The initial marine sediment deposition stage contains a package of marine–terrestrial sediments (Permian) that was deposited along a continental margin, and the marine and marine–terrestrial sediments (Yu and Guo, 2001; Zhang et al., 2006). The overlying terrestrial sediments are 1000–4000 m thick with volcanic deposits in some locations (Guo and Lei, 1998; Guo et al., 2002; Ma et al., 2004; Wu et al., 2002). After deposition and burial, an overall uplift movement since late Cretaceous in the Lower Yangtze region led to an erosion of up to 5000 m thick strata including the majority of the Mesozoic strata (Zhang et al., 2006).

The Permian strata have a total thickness of 500–1000 m, including the Qixia, Gufeng, Longtan and Dalong Formations (older to younger) (Fig. 2) with organic-rich shales within the Gufeng, Longtan and Dalong Formations (Lin et al., 2007). As reported by Liang et al. (2008), the thickness of black shales in the Gufeng Formation generally ranges from 30 to 60 m with a total organic carbon (TOC) content of 2–10 wt.%. The thickness of black shale in the Longtan Formation ranges from 100 to 200 m with an average TOC content greater than 2 wt.%. In the Dalong Formation, the shale thickness range from 20 to 50 m with a TOC content between 1 and 10 wt.% (greater than 2 wt.% on average) and occasionally reaching 21 wt.% (Liang et al., 2008). The total thickness of black shales in the Permian strata ranges from 100 to 300 m for most of the Lower Yangtze region, and can reach 600 m in the depositional center (Liang et al., 2008; Fig. 1).

3. Samples and methods

3.1. Samples

Twenty-two core samples were collected from the Middle (10 samples) and Upper (12 samples) Permian shales of two wells (C1 and H1) in the Wuhu County (Fig. 1). The two wells were drilled at the high point of two different anticline structures, and the current burial depth of Upper and Middle Permian shales ranges from 123.4 m to 341.8 m (in well C1) and from 20.1 m to 275.1 m (in well H1) (Table 1). Sample properties were determined on fresh core material and samples were selected according to the change of color in order to span a wide range of TOC contents.

3.2. Organic geochemistry and petrology

The TOC content of the shales was measured on a LECO CS-230 carbon–sulfur analyzer after removal of the carbonates by diluted hydrochloric acid according to the method by S.B. Wang et al. (2013). The TOC content was calculated by the peak area of CO_2 generated from combustion of the organic matter and calibrated by carbon in steel (TOC = 0.812 ± 0.006 wt.%).

The vitrinite reflectance (R_o) was determined on polished core samples under reflected light using a 3Y-Leica DMR XP microphotometer, according to the standard method of coal petrology as described by Dai et al. (2012). The instrument was calibrated using the cubic zirconia standard (R_o = 3.11%), and measurements were conducted in oil medium (n = 1.518) using a 50×/0.85 oil lens. In each sample, 30–50 different vitrinite particles were randomly selected for measurements and the data were averaged. In addition, eight samples were prepared

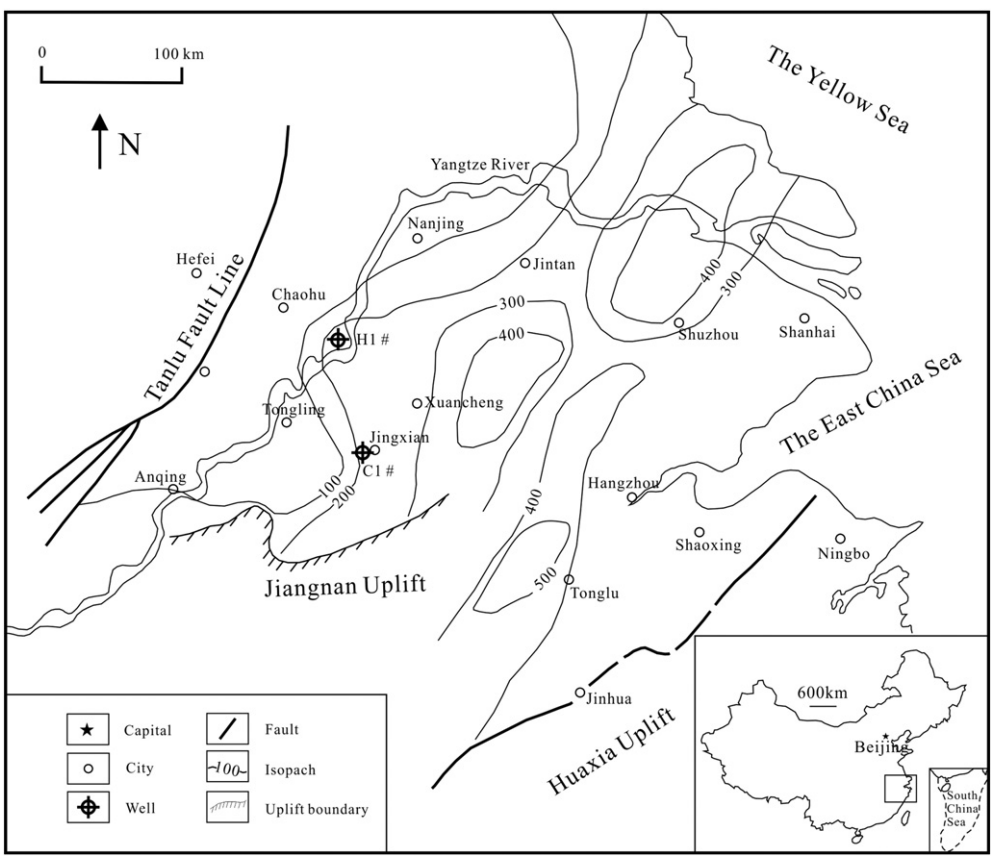

Fig. 1. Map showing the Permian shale thickness in the Lower Yangtze region in Eastern China (modified from Feng et al., 1993; Wu et al., 2013) and the locations of the two wells (C1 and H1).

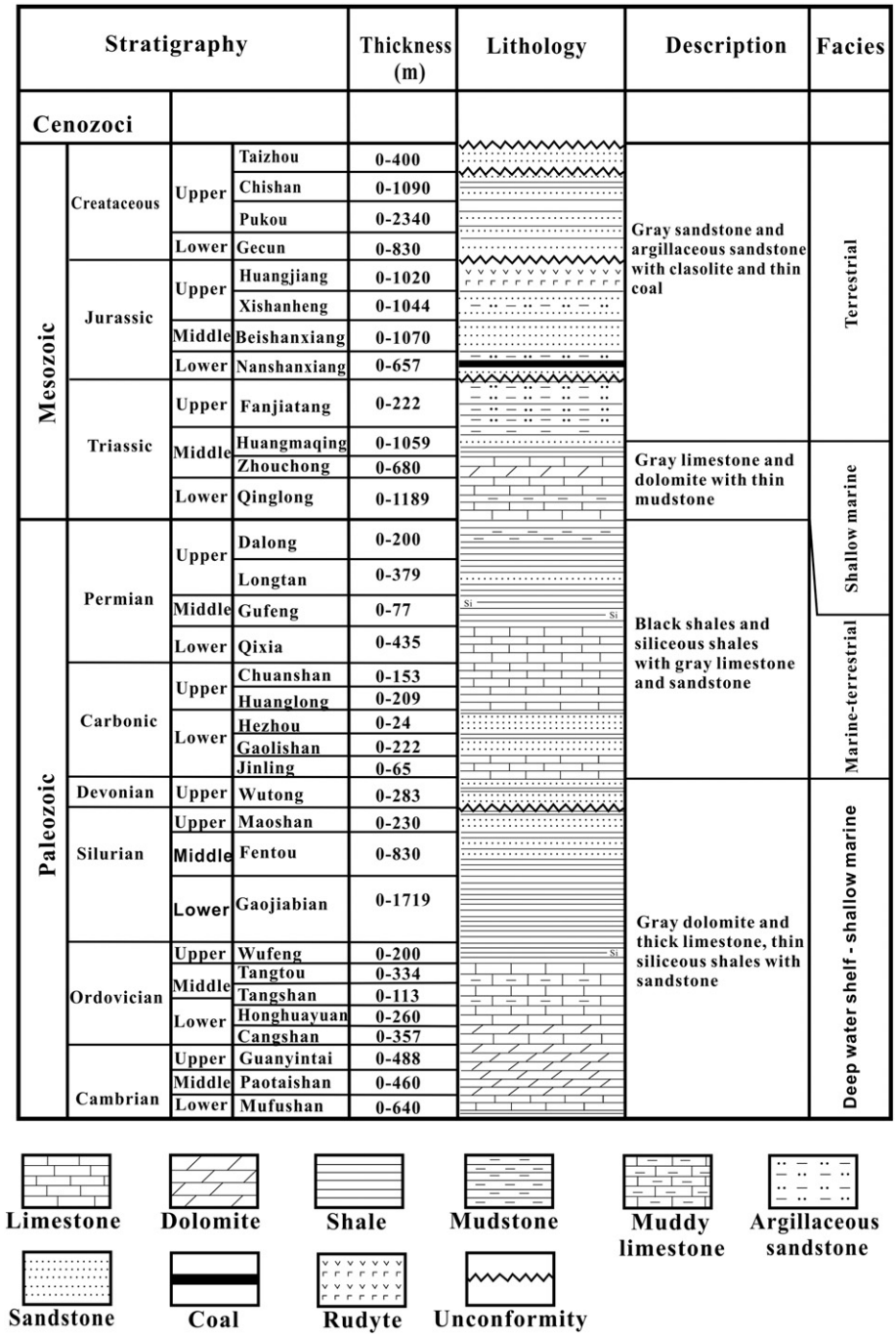

Fig. 2. Stratigraphical framework of the Lower Yangtze region (modified after Xu et al., 2011; Ji et al., 2011; Jin et al., 2013).

for kerogen typing and organic matter analysis. Maceral analyses were performed according to the methods recommended by coal petrology (GB/T 8899, 1998; Stach, 1982) and ~300 measurements were collected for each sample.

For the mineralogical composition, X-ray diffraction (XRD) analyses were carried out on shale powders using a Bruker D8 Advance X-ray diffractometer at 40 kV and 30 mA with a Cu radiation. Stepwise scanning measurements were performed at a rate of 4°/min between 3° and 85° (2θ). The mineral composition was semi-quantitatively determined (mineral wt.%) using peak area integration approach with correction for Lorentz Polarization (Pecharsky and Zavalij, 2003).

3.3. Determination of total porosity

The total porosity (φ) of the studied samples was calculated by the differences between the apparent density (ρ_a) and skeletal density (ρ_s) (Crosdale et al., 1998; G.R. Chalmers et al., 2012; Tian et al., 2013; F.Y. Wang et al., 2013):

$$\varphi = \frac{\rho_s - \rho_a}{\rho_s} \times 100\%.$$

Drilled plug samples (diameter 2.54 cm and height 4 cm) were dried at 110 °C in a vacuum for 24 h to remove free water, then weighted in air

Table 1
Depth, lithology, TOC, vitrinite reflectance (R_o) and maceral composition of the samples.

Sample no.	Depth (m)	Unit	Lithology	TOC (wt%)	R_o (%)	Maceral composition (vol %)			
						Vitrinite	Inertinite	Micrinite or amorphinite	Bitumen
C1-1	123.4	P_{3d}	Black shale	9.95	2.34	67	10	23	0
C1-2	141.2	P_{3d}	Black shale	7.82	2.36	63	13	22	2
C1-3	242.6	P_{3l}	Black shale	1.29	2.42	/	/	/	/
C1-4	261.9	P_{3l}	Black shale	1.36	2.44	/	/	/	/
C1-5	288.0	P_{3l}	Black shale	0.94	/	/	/	/	/
C1-6	305.9	P_{3l}	Black shale	3.77	2.49	77	9	10	4
C1-7	326.3	P_{2g}	Black shale	11.8	2.51	81	10	9	0
C1-8	331.1	P_{2g}	Black shale	3.67	2.48	/	/	/	/
C1-9	337.2	P_{2g}	Black shale	6.18	2.58	/	/	/	/
C1-10	341.8	P_{2g}	Black shale	8.83	2.55	/	/	/	/
H1-1	20.1	P_{3d}	Gray black shale	0.60	/	/	/	/	/
H1-2	60.5	P_{3d}	Black shale	9.20	2.44	/	/	/	/
H1-3	64.4	P_{3d}	Black shale	13.3	2.43	/	/	/	/
H1-4	74.7	P_{3d}	Black shale	15.3	2.45	79	5	12	4
H1-5	126.1	P_{3l}	Black shale	2.29	2.48	/	/	/	/
H1-6	168.6	P_{3l}	Black shale	3.51	2.51	73	10	12	5
H1-7	247.2	P_{2g}	Black shale	12.9	2.56	74	9	13	4
H1-8	252.2	P_{2g}	Black shale	9.89	2.54	/	/	/	/
H1-9	257.8	P_{2g}	Black shale	17.2	2.58	/	/	/	/
H1-10	264.2	P_{2g}	Black shale	17.4	2.61	/	/	/	/
H1-11	269.9	P_{2g}	Black shale	1.77	2.66	61	9	29	1
H1-12	275.1	P_{2g}	Black shale	12.7	2.64	/	/	/	/

P_{2g}: Gufeng Formation, P_{3l}: Longtan Formation, P_{3d}: Dalong Formations; and /: no analysis.

before and after coated by paraffin of known density, and the paraffin coated samples were finally weighted both in the air and in the water to obtain their apparent volume (Tian et al., 2013). After the analysis, the paraffin was removed and the material was crushed to powders (20–30 g) and sieved for a 20 and 40 mesh (830 and 380 μm) size fraction and then dried at 110 °C in a vacuum for 24 h. The skeletal density was measured with a helium pycnometer from Quantachrome, the Ultrapyc 1200e, at pressures less than 17.4 psi.

3.4. Low pressure adsorption

The method of low pressure nitrogen and carbon dioxide adsorption to characterize shale nanopore structures has been reported in many papers (G.R. Chalmers et al., 2012; Ross and Bustin, 2009; Strapoc et al., 2010; Tian et al., 2013). In this study, the characterization of micropore (<2 nm) and mesopore (2–50 nm) (Rouquerol et al., 1994) was investigated using the low pressure carbon dioxide and nitrogen adsorption isotherms, respectively. The adsorption experiment was carried out on an ASAP 2020 M (Micromeritics Instruments). The samples were crushed and sieved to 60–80 mesh (250–180 μm), dried in a vacuum oven at 110 °C for 24 h to remove volatile substances and free water. Low pressure N_2 adsorption is considered a standard and preferable method for surface area and pore volume measurement of mesopores (Garrido et al., 1987; Hubert and Marjo, 1996). Nitrogen adsorption isotherms were obtained at 77.4 °K with a relative pressure (P/P_o, the ratio of pressure to saturation vapor pressure) ranging from 0.005 to 0.998. The surface area was calculated using the BET equation (Brunauer et al., 1938; Gregg and Sing, 1982) and a relative pressure range between 0.05 and 0.20, and the mesopore volume was calculated using the BJH equation (Barret et al., 1951). The carbon dioxide adsorption isotherms were obtained at 273.1 °K in the relative pressure (P/P_o) range of 10^{-5}–3.2×10^{-2} (Clarkson and Bustin, 1996; Ghosal and Smith, 1996; Ross and Bustin, 2009). The micropore volume was calculated using the Dubinin–Radushkevich (D–R) equation (G.R. Chalmers et al., 2012; Clarkson and Bustin, 1996; Dubinin, 1989; Gregg and Sing, 1982; Ross and Bustin, 2009; Rouquerol et al., 1994), and the equivalent micropore surface area was calculated using the cross sectional area of the CO_2 molecule of 0.17 nm^2 (Ross and Bustin, 2009).

4. Results and discussion

4.1. Organic geochemistry and petrography

The TOC content of the samples from the two wells (C1 and H1) ranges between 0.94 and 11.8 wt.%, and 0.60 and 17.4 wt.%, respectively (Table 1). The R_o value ranges between 2.3 and 2.7% (dry gas stage). Vitrinite accounts for 61–81% of the total organic matter, with some micrinite and inertinite and small amounts of bitumen. The later three maceral groups have a content of 9–29%, 5–13% and 0–5%, respectively (Table 1). Therefore, these Permian shales are mostly gas-prone with very high maturity as previously reported from the Lower Yangtze region (Liang et al., 2009).

The mineralogical compositions of the samples are listed in Table 2 and summarized in a ternary diagram (Fig. 3). The main mineral

Table 2
Mineralogical compositions of the samples.

Sample no.	Mineralogical composition relative percent (%)							
	Quartz	Feldspar	Illite	Chlorite	Calcite	Dolomite	Pyrite	Siderite
C1-1	62.2	21.2	11.3	0.0	0.0	0.0	5.3	0.0
C1-2	45.6	15.1	31.4	0.0	3.0	0.0	4.9	0.0
C1-3	27.7	13.1	36	21.1	2.0	0.0	0.0	0.0
C1-4	30.5	10.9	37	21.6	0.0	0.0	0.0	0.0
C1-5	34.8	5.8	38.7	20.6	0.0	0.0	0.0	0.0
C1-6	56.0	0.0	36.5	0.0	0.0	0.0	7.5	0.0
C1-7	86.3	0.0	6.7	6.0	0.0	0.0	1.0	0.0
C1-8	71.7	0.0	24.6	0.0	0.0	0.0	3.7	0.0
C1-9	45.2	0.0	34.9	0.0	18.0	0.0	1.9	0.0
C1-10	32.0	0.0	28.4	8.9	17.1	4.7	6.2	2.7
H1-1	41.7	7.2	31.9	10.8	7.2	0.0	1.2	0.0
H1-2	54.8	9.5	14.3	0.0	18.1	0.0	3.2	0.0
H1-3	47.2	18.8	29.5	0.0	2.4	0.0	2.1	0.0
H1-4	51.2	15.0	29.4	0.0	0.0	0.0	4.4	0.0
H1-5	28.4	7.4	44.5	17.7	0.0	0.0	2.0	0.0
H1-6	30.2	19.9	35.2	14.7	0.0	0.0	0.0	0.0
H1-7	57.6	0.0	25.8	0.0	13.5	0.0	3.0	0.0
H1-8	62.4	0.0	24.4	0.0	8.6	0.0	4.6	0.0
H1-9	54.4	0.0	40.6	0.0	0.0	0.0	5.0	0.0
H1-10	68.8	0.0	27.8	0.0	0.0	0.0	3.4	0.0
H1-11	21.7	0.0	76.3	0.0	0.0	0.0	2.1	0.0
H1-12	67.4	0.0	20.9	0.0	0.0	0.0	6.6	5.1

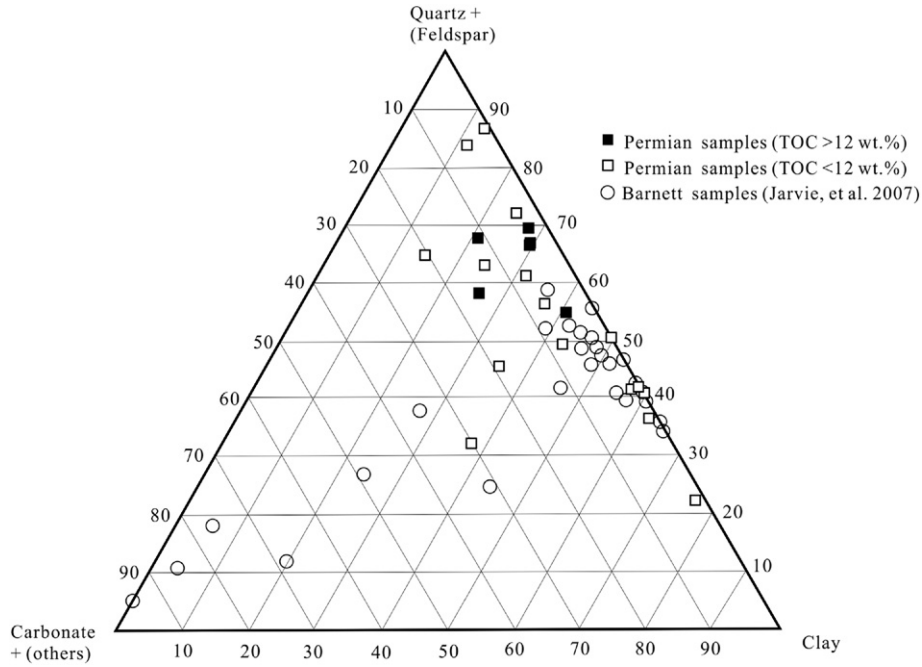

Fig. 3. Ternary diagram of quartz/feldspar, carbonate and clays of the Permian shale samples based on the normalized data from Table 2 in comparison with data from the Barnett Shale (data from Jarvie et al., 2007). The Barnett Shale samples have high carbonate contents or are 50/50 quartz–clays while most of the Permian shale samples from this study plot close to the quartz/feldspar end point or along the quartz–clay endline. The Permian samples with TOC < 12 wt.% or >12 wt.% can be identified. All samples with very high TOC contents (>12 wt.%) have elevated quartz contents.

components of the samples are quartz and clay. The quartz contents range between 21.7 and 86.3%, and the clay contents range from 11.3 to 76.3%. The clay minerals are dominated by illite with some samples also having chlorite (6–22%). Pyrite is present in most samples and is up to 6.6%. Several samples also contain up to 23% carbonates (calcite and/or dolomite), and siderite was identified in two samples (C1-10 and H1-12) (Table 2). In the ternary plot, most of the samples plot along the quartz/feldspar–clay endline towards the quartz/feldspar end member and only a few are comparable with the mineralogical composition of the Barnett Shale in the United States (Fig. 3).

G.R.L. Chalmers et al. (2012) reported a positive linear correlation between TOC and quartz contents for Devonian shale samples from the Horn River Basin in Canada ($R^2 = 0.6$, Fig. 4a) and attributed this to a significant contribution of biogenic quartz. In our study, only a weak positive correlation was observed ($R^2 = 0.38$, Fig. 4a). This would be owing to the change of sedimentary facies (marine–terrestrial transition) of the studied samples. The relationship between TOC and clay contents seems more inconclusive (Fig. 4b). A negative correlation is observed for samples with TOC < 12 wt.%, whereas a positive correlation exists for samples with higher TOC. Therefore, more data are needed to fully understand the relationship between TOC and clay mineral contents in these shales.

4.2. Total porosity and controlling factors

The skeletal density, apparent density and total porosity of the samples are listed in Table 3 and their relationships with TOC are presented in Fig. 5. With increasing TOC content, the skeletal density decreases linearly with a coefficient of 0.9 (Fig. 5a), which is likely due to density differences (i.e. organic matter about 1.4 g/cm^3 and minerals about 2.70 g/cm^3) (Ross and Bustin, 2008). The apparent densities of the samples also decrease with increasing TOC content with a multinomial correlation ($R^2 = 0.94$, Fig. 5a). The reduction in apparent density tends to be less for samples with TOC > 12 wt.%, which implies that other factors may influence density of the higher TOC samples. The correlation between total porosity and TOC content shows a positive linear relationship when TOC < 12 wt.% and a negative relationship when TOC > 12 wt.% (Fig. 5b). This unusual pattern was also reported by Milliken et al. (2013) for the Marcellus shales, but a cause is not obvious.

Total porosity of gas shales includes inorganic matrix porosity and organic porosity (G.R. Chalmers et al., 2012; Curtis et al., 2012; Mastalerz et al., 2013; Milliken et al., 2012). The inorganic matrix porosity is mainly controlled by diagenesis and compaction, presenting a simple reduction model with increasing burial depth (Cander, 2012; F.Y. Wang et al., 2013), whereas the evolution of organic porosity has not been well defined owing to the lack of data (Cander, 2012; Chen and Xiao, 2014; Mastalerz et al., 2013; Milliken et al., 2013; F.Y. Wang et al., 2013). For a general understanding, contribution of per gram organic carbon to total porosity (calculation from the linear regression relation between TOC and total porosity) for some shales with different maturities is presented here. The contribution is about 0.84% for the Mowry shales with a R_o value of 1.5–1.6% (Modica and Lapierre, 2012) and about 1.2–1.4% for the Marcellus shales with a R_o value of 1–2.1% (Milliken et al., 2013). The contribution is 0.72% for the Lower Silurian shale in Southern China with an equivalent vitrinite reflectance (EqR_o) of 2.5–3.0% (Tian et al., 2013), and 0.4% for the Lower Cambrian shale in Southern China with an EqR_o of 2.5–3.6% (F.Y. Wang et al., 2013). According to these data, the contribution of per gram organic matter to total porosity is decreasing with increasing maturation for very high maturity shales (R_o > 2.0%), which is attributed to increasing compaction (F.Y. Wang et al., 2013). The influence of this compaction on total porosity is also related to the TOC content as well as organic matter type. Milliken et al. (2013) noticed that the increase of total porosity with the TOC content turns to be at a diminished rate, even their relationship is reverse for the Marcellus shales with a high TOC content (>5.5 wt.%), which may be attributed to pore collapse during gas expulsion and greater organic matter connectivity and framework compaction or organic matter with lower initial hydrogen index in contrast to samples with lower TOC (<5.5 wt.%) (Milliken et al., 2013).

The R_o values of the Permian samples vary within a very narrow range of 2.3–2.7% (Table 1) indicating a similar thermal maturation (gas-window). Hence, variability in total porosity could be influenced by a combination factors including TOC content, OM type or mineral

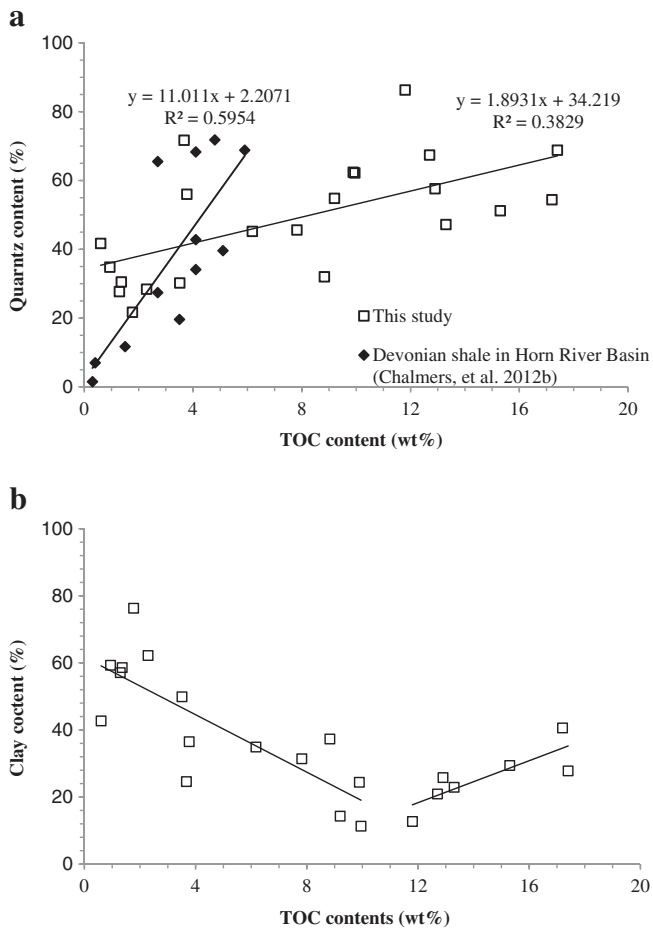

Fig. 4. Plot showing the relationship of the Permian samples between quartz and TOC contents in comparison with the Devonian shales in the Horn River Basin in Canada (data from Chalmers et al., 2012b) (a), and the relationship between TOC and clay mineral contents of the samples (b). A negative correlation for samples with TOC < 12 wt.% and a positive correlation for samples with TOC > 12 wt.% are observed.

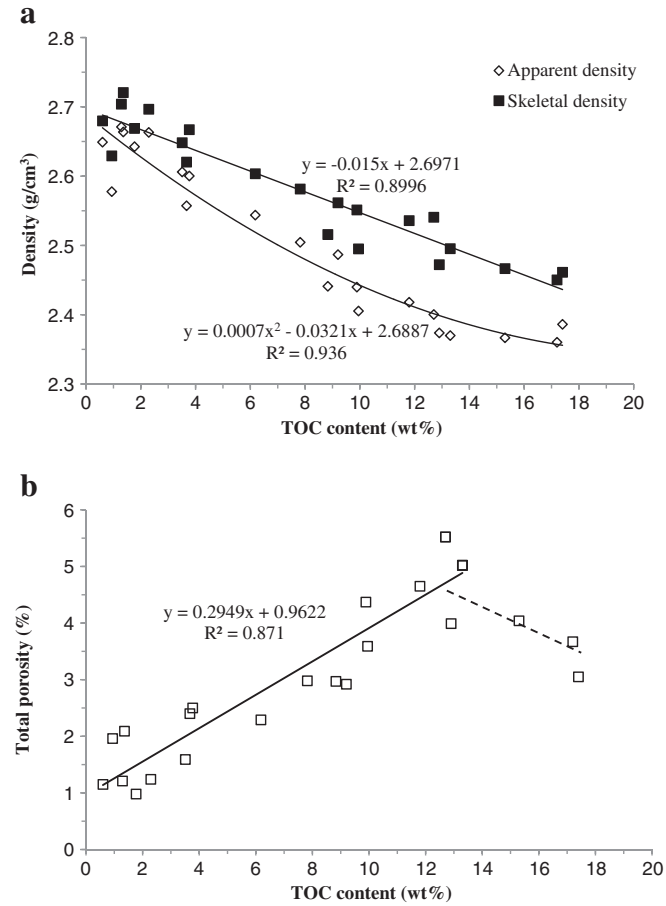

Fig. 5. Plots showing the relationships between TOC and the skeletal and apparent densities (a), and the relationship between TOC and total porosity (b) of the samples.

composition. For samples with TOC < 12 wt.%, their average inorganic porosity is about 0.96% by extrapolating the linear regression to zero TOC (Tian et al., 2013), similar to the high mature Marcellus

Table 3
Apparent and skeletal density, total porosity, and pore structure data of the samples.

Sample no.	Apparent density/g cm^{-3}	Skeletal density/g cm^{-3}	Porosity/%	BET specific surface area/m^2 g^{-1}	Mesopore volume/cm^3 100 g^{-1}	Mesopore surface area/m^2 g^{-1}	Mean pore size/nm	CO_2 micropore volume/cm^3 100 g^{-1}	CO_2 equivalent micropore surface area/m^2 g^{-1}
C1-1	2.4053	2.4950	3.59	17.91	1.03	5.96	9.4	0.79	19.67
C1-2	2.5045	2.5814	2.98	17.61	1.19	7.60	8.2	0.70	17.35
C1-3	2.6710	2.7039	1.21	8.07	0.86	4.95	13.6	0.37	8.81
C1-4	2.6637	2.7206	2.09	9.61	0.97	6.21	12.4	0.38	9.59
C1-5	2.5776	2.6292	1.96	10.09	0.94	5.74	12.6	0.39	9.59
C1-6	2.6002	2.6670	2.50	13.78	1.00	6.78	9.6	0.51	12.72
C1-7	2.4180	2.5358	4.65	18.24	1.29	8.62	9.1	0.80	20.03
C1-8	2.5572	2.6202	2.40	10.08	0.67	5.96	10	0.34	8.53
C1-9	2.5437	2.6034	2.29	14.08	0.96	5.87	9.3	0.47	11.8
C1-10	2.4410	2.5157	2.97	19.77	1.24	8.15	8.5	0.66	16.54
H1-1	2.6490	2.6797	1.15	5.94	0.84	3.59	14.5	0.22	5.41
H1-2	2.4867	2.5615	2.92	16.65	0.95	7.17	7.8	0.87	21.70
H1-3	2.3699	2.4953	5.02	20.59	1.61	10.83	8.3	1.28	31.79
H1-4	2.3667	2.4665	4.04	23.42	1.60	11.01	7.8	1.32	32.82
H1-5	2.6631	2.6965	1.24	8.84	0.87	5.50	11.7	0.46	11.51
H1-6	2.6060	2.6482	1.59	10.32	0.77	5.77	11.3	0.52	13.04
H1-7	2.3737	2.4722	3.99	19.72	1.25	9.20	6.5	1.07	26.66
H1-8	2.4398	2.5512	4.37	22.01	1.21	9.81	8.4	1.02	25.51
H1-9	2.3602	2.4502	3.67	23.56	1.44	11.23	6.7	1.44	35.69
H1-10	2.3861	2.4612	3.05	21.67	1.23	10.73	5.8	1.29	32.01
H1-11	2.6425	2.6688	0.98	8.69	1.01	5.31	13.6	0.35	8.87
H1-12	2.4003	2.5406	5.52	24.38	1.76	10.80	8.5	0.97	24.22

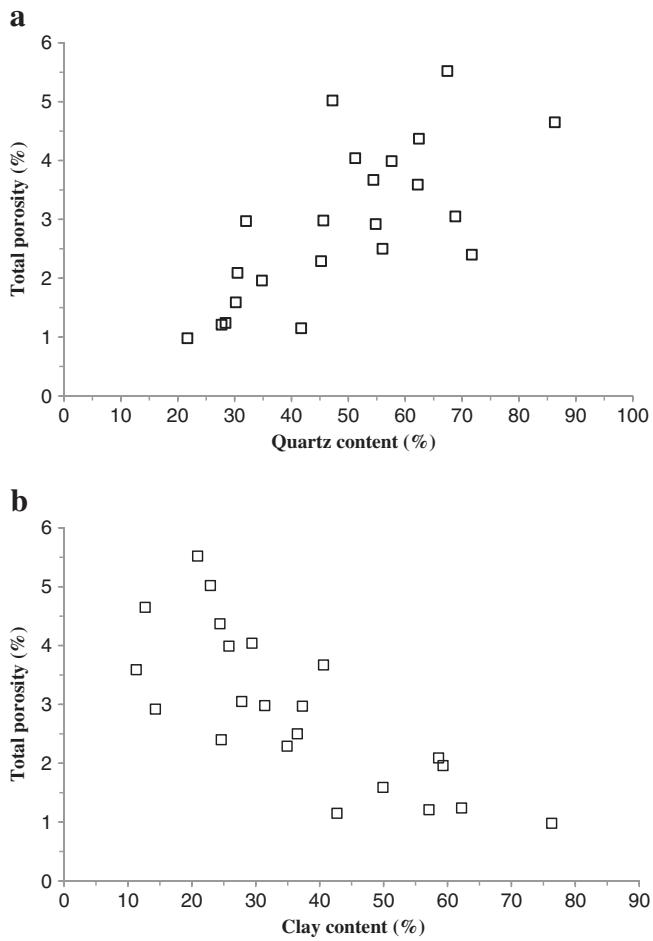

Fig. 6. Plots showing the relationships between quartz content and total porosity (a) as well as between clay content and total porosity (b) of the samples.

shales (about 1.0%) (Milliken et al., 2013) as well as Lower Cambrian shales in Southern China (about 1.1–1.2%) (F.Y. Wang et al., 2013), which indicates that the lithological variability of shales with a very high maturity has a much low controlling effect on their porosity than does their TOC content. However, the contribution of per gram organic matter to the total porosity is only 0.29% for samples with TOC < 12 wt.%, which is significantly lower than that of the Lower Silurian shales (with dominated oil-prone kerogen) with a similar maturity (Tian et al., 2013; F.Y. Wang et al., 2013). The less development of organic porosity of the Permian samples may be related to their dominated gas-prone organic matter which has a smaller volume loss associated with devolatilization during maturation (Milliken et al., 2013). The decrease of total porosity with increasing TOC for samples with higher TOC contents (>12 wt.%) may be also interpreted by pore collapse similar to the case of the Marcellus shales (Milliken et al., 2013) since their mineralogical compositions and organic matter types are not significantly different from the samples with a lower TOC content from the available data (Tables 1, 2, Fig. 3).

The relationships of total porosity, quartz and clay minerals are shown in Fig. 6. Total porosity is positively correlated with quartz content in the range between 20 and 60%, but if quartz content is >60% the data becomes scattered (Fig. 6a). Although biogenic quartz may contain some intraparticle pores (G.R.L. Chalmers et al., 2012; Ross and Bustin, 2009), it is unlikely the main reason for elevated porosity since TOC content increases with increasing quartz content (Fig. 4a). The correlation of total porosity with quartz content actually mainly reflects the relationship between TOC content and total porosity. Although clay minerals contribute to total porosity (Chalmers and Bustin, 2008; G.R. Chalmers et al., 2012; Curtis et al., 2010), the total porosity is negatively related to the clay contents, indicating that in these samples, the contribution to total porosity is negligible. The explanations about these relationships are preliminary and need to be confirmed with future investigations and details about sedimentological and compositional (including diagenetic) variability within the studied strata.

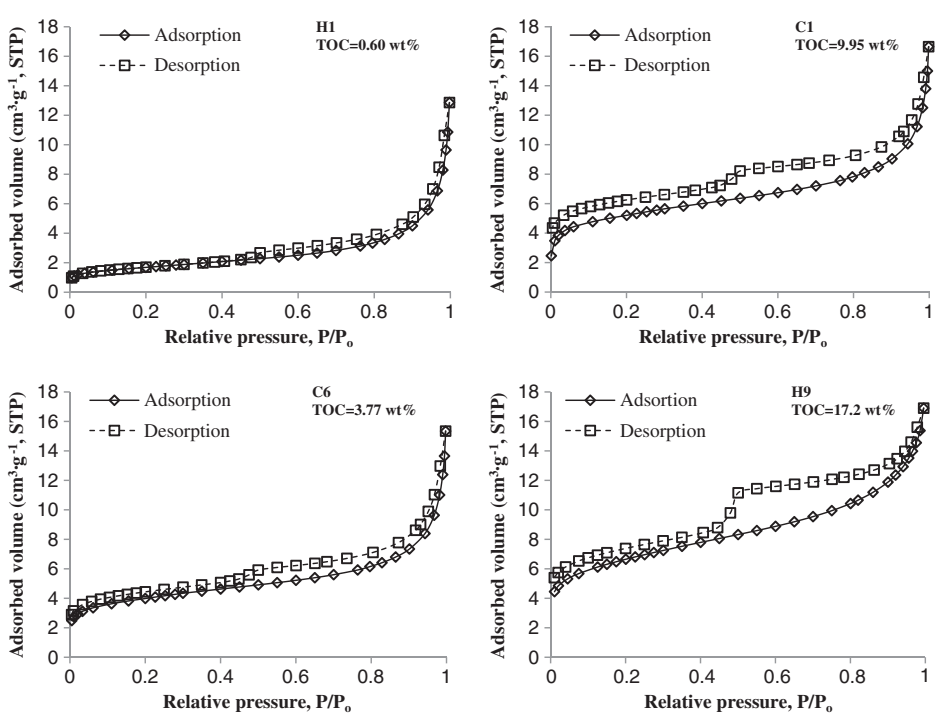

Fig. 7. Nitrogen adsorption–desorption isotherms (77.4 °K) of the selected samples from the two wells. The hysteresis loop becomes more defined with increasing TOC content.

4.3. Nanopore structure and the controlling factors

Nanometer-size pores (i.e. nanopores) are abundant in shale deposits. Organic matter is assumed to be the main sites of nanopores in organic-rich shales (G.R. Chalmers et al., 2012; Loucks et al., 2009; Schieber, 2011; Slatt and O'Brien, 2011). The isotherm of nitrogen adsorption for the samples is quite similar to the type II isotherm defined by the International Union of Pure and Applied Chemistry (Ross and Bustin, 2008; Rouquerol et al., 1994; Sing et al., 1985) with the type H3 hysteresis loop, which becomes more defined with increasing TOC content (Fig. 7). The carbon dioxide adsorption isotherm shape for the samples is similar to that of coals reported by Clarkson and Bustin (1996), but the adsorption capacity of the shales is far less than coals. The capacity of the CO_2 adsorption below atmosphere pressure is mainly related to the micropore volume and less controlled by the surface area (Sing et al., 1985). The adsorption amount of CO_2 on the samples is positively correlated with the TOC content (Fig. 8), implying that the organic matters contain abundant micropores (for gas storage).

The specific surface area and volume of micropores and mesopores of the studied shales are listed in Table 3. The BET total specific surface area and mesopore specific surface range between 5.94–24.38 m^2/g and 3.59–11.23 m^2/g, respectively. The mesopore volume ranges between 0.67 and 1.76 $cm^3/100$ g. The micropore volume ranges between 0.22 and 1.44 $cm^3/100$ g, and the micropore specific surface area ranges between 5.41 and 35.69 m^2/g. The BET total surface area shows a positive correction with the micropore volume (Fig. 9), implying that a significant portion of the total surface area is contributed by micropore. Both the micropore volume and specific surface area are positively correlated with TOC (Fig. 10a,b). Similar positive relationships exist between TOC, mesopore volume and specific surface area for samples with TOC < 12 wt.% (Fig. 10a,b), but the increase of the surface area becomes slower and the volume even turns to decrease with further increasing TOC content (Fig. 10a,b).

Nanopores associated with clay minerals are generally bigger than these in organic matter, and pores in clay minerals range mainly between mesopores and macropores (Chalmers and Bustin, 2008; G.R. Chalmers et al., 2012; Curtis et al., 2010). Pore volume and specific surface areas of clay minerals decreases with increasing maturity owing to the dehydration and microstructural change during diagenesis (Helen et al., 1998; Chen and Xiao, 2014). In the Permian samples, the micropore and mesopore specific surface areas, and the micropore and mesopore volumes show little trends against clay content (Fig. 11). This implies that clay minerals in the studied samples are not the main factor governing the nanopore structure.

Although the samples are recovered from shallow depths (<350 m), the thermal maturity of the organics suggest elevated diagenetic overprint and hence sediment compaction (Yu and Guo, 2001; Zhang et al., 2006), which results in a very low inorganic matrix porosity (0.96%, Fig. 6b). From the above discussion, the decrease of total porosity with increasing TOC for the higher TOC samples (Fig. 5a) is due to the decrease of macropore and mesopore volume mainly in organic matters which should be also attributed to this diagenetic compaction. The mean pore size value of the samples ranges between 6 and 15 nm and has a slight negative correlation with TOC ($R^2 = 0.79$, Fig. 12), which

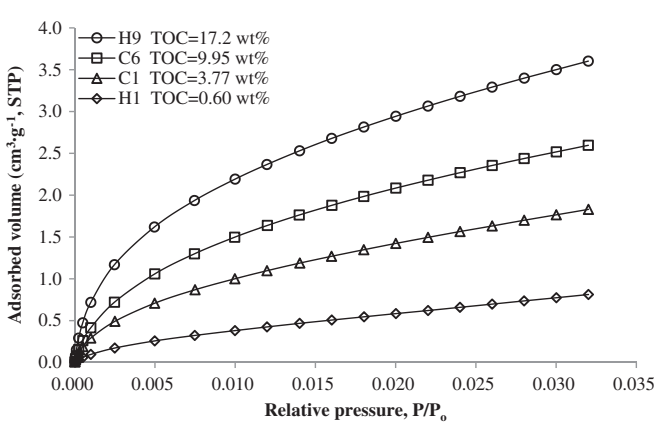

Fig. 8. CO_2 adsorption isotherms (273.1 °K) of the selected samples. The adsorbed volume increases in samples with higher TOC content.

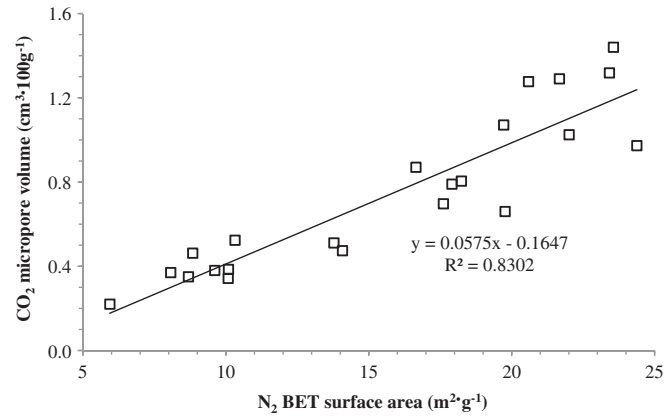

Fig. 9. Plot showing the relationship between CO_2 micropore volume and N_2 BET surface area of the samples.

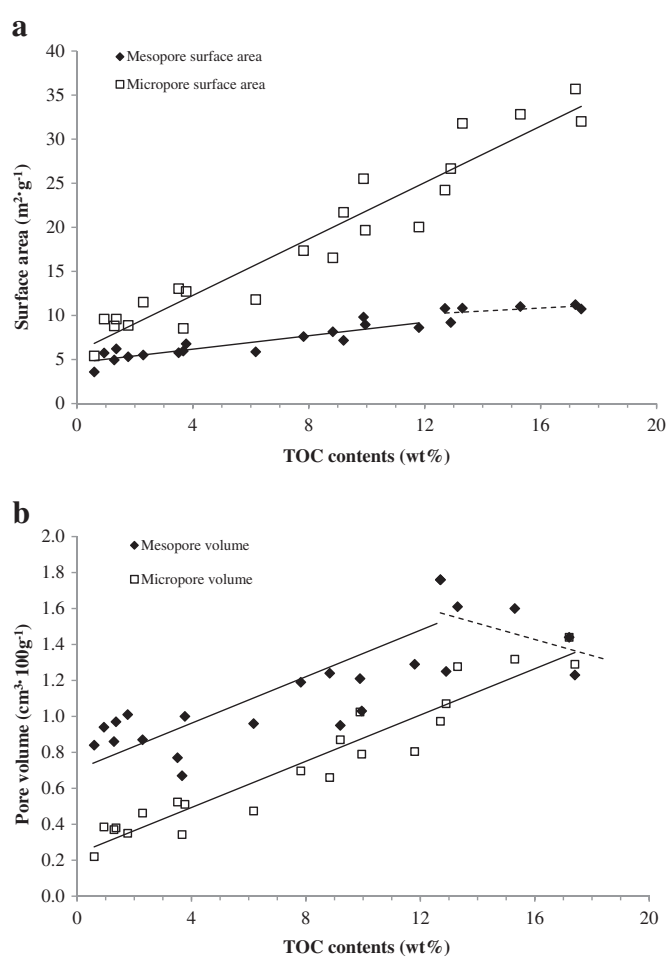

Fig. 10. Plots showing the relationships of TOC and specific surface areas (a) and TOC and pore volumes (b) of the samples.

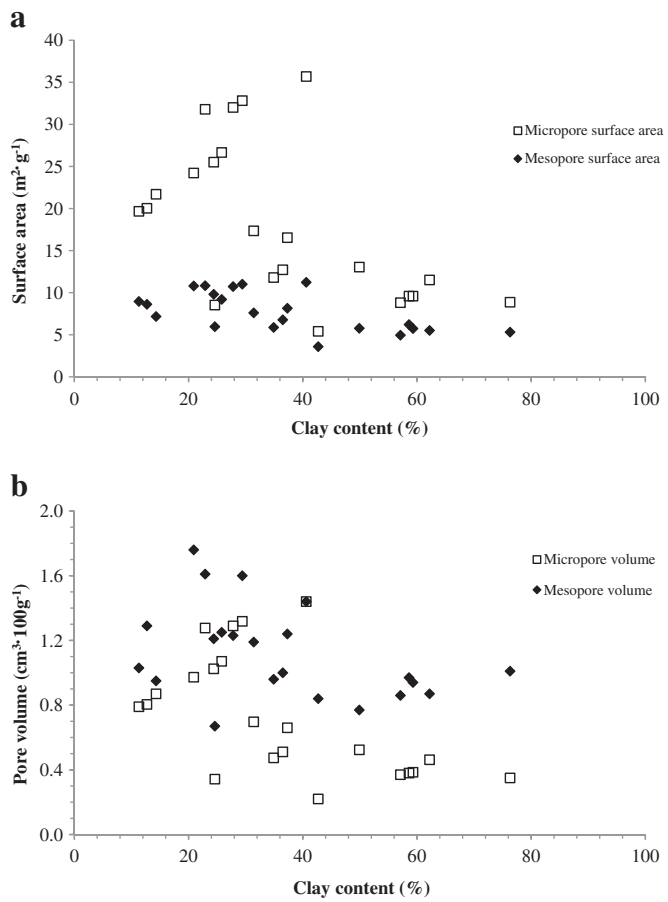

Fig. 11. Plots showing the relationships of clay content and specific surface areas (a) and clay content and pore volume (b) of the samples.

indicates that in general, smaller pores dominate samples with elevated TOC contents.

4.4. Shale gas potential

Shale gas exists in three forms: free gas in pores and fractures, adsorbed gas on surface area of organic matter and clay minerals, and dissolved gas in oil and water (Clarkson and Bustin, 1996; Curtis, 2002; Hao and Zou, 2013; Zhang et al., 2008; T.W. Zhang et al., 2012). In shales with very high maturity, free and adsorbed gases are dominant with very low contents of dissolved gas (Curtis, 2002; Zhou et al., 2013).

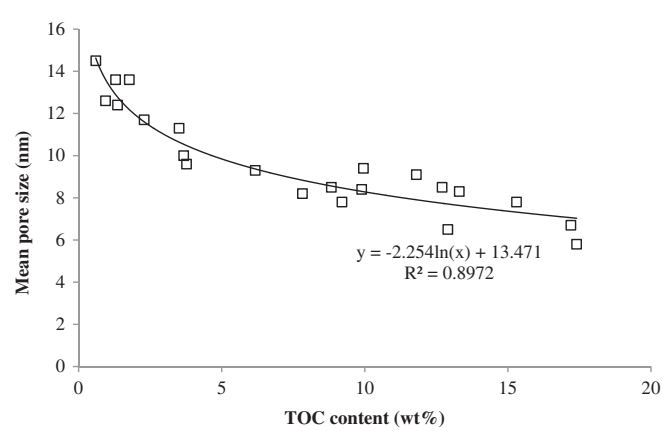

Fig. 12. Plot showing the relationship between TOC and mean pore size (in 1.7–300 nm) of the samples. An overall decreasing mean pore size is observed with increasing TOC.

While free gas occurs mainly in macropores and larger mesopores, adsorbed gas is located mainly within micropores as well as at surface of mesopores and macropores (Montgomery et al., 2005; Hill et al., 2007; Ross and Bustin, 2008; G.R. Chalmers et al., 2012; Huang et al., 2012b; Mosher et al., 2013). In the Permian samples, it appears that the organic matter mostly controls porosity and nanopore structure, thus influencing storage capacity and occurrence of the gas.

The study shows that the samples with low TOC (<4 wt.%) have total porosity <2% and micropore surface area <13 m^2/g, thus indicating lower free gas and adsorbed gas. Samples with TOC between 4 and 12 wt.% have total porosity of 2–5% and micropore surface area of 12–25 m^2/g, and the gas storage capacity for both free and adsorbed phases increases with increasing TOC. Samples with high TOC (>12 wt.%) have total porosity of 3–5% and micropore surface area of 23–36 m^2/g, implying a somewhat similar amount of free gas but an increase of adsorbed gas.

5. Conclusion

The geochemistry, porosity and pore structure of 22 Permian shales from the Lower Yangtze region were investigated and the following preliminary conclusions are drawn.

(1) The organic matter is dominated by gas-prone kerogen with TOC contents ranging between 0.6 and 17.4 wt.% and thermal maturity (vitrinite reflectance or R_o) values of 2.3–2.7% with an average of 2.5%. The mineralogical composition is dominated by quartz and clays with some samples having feldspars and carbonates and small amounts of pyrite.
(2) Samples with TOC < 12 wt.% have a positive liner correlation with total porosity while samples with TOC > 12 wt.% have a negative correlation. This may be due to stronger framework compaction in samples with very high (>12 wt.%) TOC.
(3) The micropore volume and surface area as well as mesopore surface area for the all samples, and the mesopore volumes for samples with TOC < 12 wt.% display positive correlations with TOC content, whereas the mesopore volumes for the higher TOC samples are negatively correlated with TOC content. This may imply that larger organic matter-hosted pores in the high TOC samples underwent elevated compaction.
(4) The TOC content is the key factor to control gas storage capacity of the Permian shales in Lower Yangtze region.

Acknowledgments

The authors are indebted to two anonymous reviewers for their insightful comments and suggestions that have significantly improved the manuscript. Special acknowledgements are given to Dr. R. W. T. Wilkins for assistance with English. This study was supported by the National Key Basic Research Program of China (973 Program: 2012CB214705), a special program of Chinese Academy of Science (XDB10040300), and the National Natural Science Foundation of China (41321002).

References

Barret, E.P., Joyner, L.G., Halenda, P.P., 1951. The determination of pore volume and area distribution in porous substances. I. Computations from nitrogen isotherms. J. Am. Chem. Soc. 73 (1), 373–380.
Brunauer, S., Emmett, P.H., Teller, E., 1938. Adsorption of gases in multimolecular layers. J. Am. Chem. Soc. 60 (2), 309–319.
Cander, H., 2012. Sweet spots in shale gas and liquids plays: prediction of fluid composition and reservoir pressure. AAPG Annual Convention and Exhibition, Long Beach, California, April 22–25.
Chalmers, G.R., Bustin, R.M., 2008. Lower Cretaceous gas shales in northeastern British Columbia, Part I: geological controls on methane sorption capacity. Bull. Can. Pet. Geol. 56 (1), 1–21.

Chalmers, G.R., Bustin, R.M., Power, I.M., 2012a. Characterization of gas shale pore systems by porosimetry, pycnometry, surface area, and field emission scanning electron microscopy/transmission electron microscopy image analyses: examples from the Barnett, Woodford, Haynesville, Marcellus, and Doig units. AAPG Bull. 96 (6), 1099–1119.

Chalmers, G.R.L., Ross, D.J.K., Bustin, R.M., 2012b. Geological controls on matrix permeability of Devonian Gas Shales in the Horn River and Liard basins, northeastern British Columbia, Canada. Int. J. Coal Geol. 103, 120–131.

Chen, J., Xiao, X.M., 2014. Evolution of nanoporosity in organic-rich shales during thermal maturation. Fuel 129, 173–181.

Chen, P., Zhang, M.Q., Xu, Y.Z., Liu, J.S., Du, X.B., Hu, X.H., Lu, Y.C., 2013. The shale reservoir characteristic of Dalong Formation Upper Permian in Chaohu-Jingxian, Lower Yangtze area. Acta Pet. Sin. 29 (8), 2925–2935 (in Chinese with English abstract).

Clarkson, C.R., Bustin, R.M., 1996. Variation in micropore capacity and size distribution with composition in bituminous coal of the Western Canadian Sedimentary Basin: implications for coalbed methane potential. Fuel 75 (13), 1483–1498.

Crosdale, P.J., Beamish, B.B., Valix, M., 1998. Coalbed methane sorption related to coal composition. Int. J. Coal Geol. 35 (1 ~ 4), 147–158.

Curtis, J.B., 2002. Fractured shale-gas systems. AAPG Bull. 86 (11), 1921–1938.

Curtis, M.E., Ambrose, R.J., Sondergeld, C.H., Rai, C.S., 2010. Structural characterization of gas shale on the micro- and nano-scales. Soc. Petrol. Eng. (SPE 137693) 1–15.

Curtis, M.E., Cardott, B.J., Sondergeld, C.H., Rai, C.S., 2012. Development of organic porosity in the Woodford Shale with increasing thermal maturity. Int. J. Coal Geol. 103, 26–31.

Dai, S.F., Zou, J.H., Jiang, Y.F., Ward, C.R., Wang, X.B., Li, T., Xue, W.F., Liu, S.D., Tian, H.M., Sun, X.H., Zhou, D., 2012. Mineralogical and geochemical compositions of the Pennsylvanian coal in the Adaohai Mine, Daqingshan Coalfield, Inner Mongolia, China: modes of occurrence and origin of diaspore, gorceixite, and ammonian illite. Int. J. Coal Geol. 94, 250–270.

Ding, D.G., Li, P., Lu, J.X., 1987. The prototypes of late Paleozoic petroliferous basins in lower section area of Yangtze River. Exp. Pet. Geol. 9 (3), 272–282 (in Chinese with English abstract).

Du, X.D., Huang, Z., Chen, Z.N., Liu, J.R., 1999. Division and correlation of the Permian sequence in Lower Yangtze region. J. Stratigr. 23, 152–160 (in Chinese with English abstract).

Du, Y.L., Li, S.Y., Wan, Q., Li, H.X., 2010. The Permian sedimentary facies and depositional environment analysis in the Jingxian-Nanling region of Anhui. J. Stratigr. 34 (4), 431–444 (in Chinese with English abstract).

Dubinin, M.M., 1989. Fundamentals of the theory of adsorption in micropores of carbon adsorbents: characteristics of their adsorption properties and microporous structures. Carbon 27 (3), 457–467.

Feng, Z.Z., He, Y.B., Wu, S.H., 1993. Listhofacies paleogeography of Permian Middle and Lower Yangtze region. Acta Sedimentol. Sin. 11 (3), 13–24 (in Chinese with English abstract).

Garrido, J., Linares-Solano, A., Mardn-Mardnez, J.M., Molina-Sabio, M., Rodriguez-Reinoso, F., Torregrosa, R., 1987. Use of nitrogen vs. carbon dioxide in the characterization of activated carbons. Langmuir 3 (1), 76–81.

GB/T 8899, 1998. Determination of Maceral Group Composition and Minerals in Coal.

Ghosal, R., Smith, D.M., 1996. Micropore characterization using the Dubinin–Astakhov equation to analyze high pressure CO_2 (273 K) adsorption data. J. Porous. Mater. 3, 247–255.

Gregg, S.J., Sing, K.S.W., 1982. Adsorption, Surface Area and Porosity. 2nd edition. Academic Press, New York, p. 303.

Guo, N.F., Lei, Y.X., 1998. Evaluation on the geologic conditions of the Mesozoic hydrocarbons in the Lower Yangtze Area. Exp. Pet. Geol. 20 (4), 354–361 (in Chinese with English abstract).

Guo, T.L., Zhang, H.R., 2014. Formation and enrichment model of Jiaoshiba shale gas field in Sichuan Basin. Pet. Explor. Dev. 41 (1), 28–36 (in Chinese with English abstract).

Guo, N.F., You, X.Z., Liu, D.F., 1998. Palaeozoic oil and gas geological conditions and exploration area screening in Lower Yangzi region. Pet. Explor. Dev. 25 (4), 4–9 (in Chinese with English abstract).

Guo, N.F., Zhao, H.G., Chen, H., Zhang, W., Zhao, X.H., 2002. Oil–gas occurrence conditions and evaluation of chosen belts of the marine strata in Yangtze Area. J. Northwest Univ. (Nat. Sci. Ed.) 32 (5), 526–530 (in Chinese with English abstract).

Hao, F., Zou, H.Y., 2013. Cause of shale gas geochemical anomalies and mechanisms for gas enrichment and depletion in high-maturity shales. Mar. Pet. Geol. 44, 1–12.

Helen, J.B., Redfern, S.A.T., Clark, S.M., 1998. The kinetics of dehydration in Ca-montmorillonite: an in situ X-ray diffraction study. Mineral. Mag. 62 (5), 647–656.

Hill, R.J., Zhang, E., Katz, B.J., Tang, Y.C., 2007. Modeling of gas generation from the Barnett Shale, Fort Worth Basin, Texas. AAPG Bull. 91 (4), 501–521.

Huang, J.L., Zou, C.N., Li, J.Z., Dong, D.Z., Wang, S.J., Wang, S.Q., Cheng, K.M., 2012a. Shale gas generation and potential of the Lower Cambrian Qiongzhusi Formation in the Southern Sichuan Basin, China. Pet. Explor. Dev. 39 (1), 75–81.

Huang, J.L., Zou, C.N., Li, J.Z., Dong, D.Z., Wang, S.J., Wang, S.Q., Wang, Y.M., Li, D.H., 2012b. Shale gas accumulation conditions and favorable zones of Silurian Longmaxi Formation in south Sichuan Basin, china. J. China Coal Soc. 37 (5), 782–787.

Hubert, D.J., Marjo, C.M.H., 1996. Adsorption of CO_2 and N_2 on soil organic matter: nature of porosity, surface Area, and diffusion mechanisms. Environ. Sci. Technol. 30 (2), 408–413.

Jarvie, D.M., Hill, R.J., Ruble, T.E., Pollastro, R.M., 2007. Unconventional shale-gas systems: the Mississippian Barnett shale of north-central Texas as one model for thermogenic shale-gas assessment. AAPG Bull. 91 (4), 475–499.

Ji, Y.L., Zhou, Y., Wang, G.W., Lu, L.L., 2011. Sequence stratigraphic models and reservoir prediction of the Paleozoic marine carbonates in the Lower Yangtze area. Oil Gas Geol. 32 (54), 724–732 (in Chinese with English abstract).

Jin, Z.J., Liu, G.X., Fang, C.M., Zhang, C.J., Peng, J.N., 2013. Evaluation of selected areas for petroleum exploration in marine strata of Lower Yangtze region. Pet. Geol. Exp. 35 (5), 473–479 (in Chinese with English abstract).

Liang, D.G., Guo, T.L., Chen, J.P., Bian, L.Z., Zhao, Z., 2008. Some progresses on studies of hydrocarbon generation and accumulation in marine sedimentary regions, Southern China (Part 1): distribution of four suits of regional marine source rocks. Mar. Orig. Pet. Geol. 13 (2), 1–16 (in Chinese with English abstract).

Liang, D.G., Guo, T.L., Chen, J.P., Bian, L.Z., Zhao, Z., 2009. Some progresses on studies of hydrocarbon generation and accumulation in marine sedimentary regions, Southern China (Part 2): geochemical characteristics of fore suits of regional marine source rocks, South China. Mar. Orig. Pet. Geol. 14 (1), 1–15 (in Chinese with English abstract).

Lin, X.Y., Liu, J., Chen, Z.L., He, L.L., Shen, L.C., 2007. Marine source rock distribution and hydrocarbon generation potential in middle and lower Yangtze region. J. Oil Gas Technol. 29 (3), 15–19 (in Chinese with English abstract).

Loucks, R.G., Reed, R.M., Ruppel, S.C., Jarvie, D.M., 2009. Morphology, genesis, and distribution of nanometer-scale pores in siliceous mudstones of the Mississippian Barnett Shale. J. Sediment. Res. 79, 848–861.

Ma, L., Chen, H.J., Gan, K.W., Xu, K.D., Xu, X.S., Wu, G.Y., Ye, Z., Liang, X., Wu, S.H., Qiu, Y.Y., Zhang, P.L., Ge, P.P., 2004. Tectonic and marine oil and gas geology in Southern China. Geology Publishing House, Beijing (in Chinese).

Mastalerz, M., Schimmelmann, A., Drobniak, A., Chen, Y.Y., 2013. Porosity of Devonian and Mississippian New Albany Shale across a maturation gradient: insights from organic petrology, gas adsorption, and mercury intrusion. AAPG Bull. 97 (10), 1621–1643.

Milliken, K.L., Esch, W.L., Reed, R.M., Zhang, T.W., 2012. Grain assemblages and strong diagenetic overprinting in siliceous mudrocks, Barnett Shale (Mississippian), Fort Worth Basin, Texas. AAPG Bull. 96 (9), 1553–1578.

Milliken, K.L., Rudnicki, M., Awwiller, D.N., Zhang, T.W., 2013. Organic matter-hosted pore system, Marcellus Formation (Devonian), Pennsylvania. AAPG Bull. 97 (2), 177–200.

MLRC (Ministry of Land and Resources of the People's Republic of China), 2014. The first large-scale shale gas field of China is advance into commercial development. http://www.mlr.gov.cn/xwdt/jrxw/201403/t20140327130928 6.htm.

Modica, C.J., Lapierre, S.G., 2012. Estimation of kerogen porosity in source rocks as a function of thermal transformation: example from the Mowry Shale in the Powder River Basin of Wyoming. AAPG Bull. 96 (1), 87–108.

Montgomery, S.L., Jarvie, D.M., Bowker, K.A., Pollastro, R.M., 2005. Mississippian Barnett Shale, Fort Worth basin, north-central Texas: Gas-shale play with multi-trillion cubic foot potential. AAPG Bull. 89 (2), 155–175.

Mosher, K., He, J.J., Liu, Y.Y., Rupp, E., Wilcox, J., 2013. Molecular simulation of methane adsorption in micro- and mesoporous carbons with applications to coal and gas shale systems. Int. J. Coal Geol. 109–110, 36–44.

Pan, J.P., Qiao, D.W., Li, S.Z., Zhou, D.S., Xu, L.F., Zhang, M.Y., Song, X.Y., 2011. Shale-gas geological conditions and exploration prospect of the Paleozoic marine strata in lower Yangtze area, China. Geol. Bull. China 30 (2 ~ 3), 337–343 (in Chinese with English abstract).

Pecharsky, V.K., Zavalij, P.Y., 2003. Fundamentals of Powder Diffraction and Structural Characterization of Minerals. Kluwer Academic Publishers, New York, p. 713.

Ross, D.J.K., Bustin, R.M., 2008. Characterizing the shale gas resource potential of Devonian–Mississippian strata in the Western Canada sedimentary basin: application of an integrated formation evaluation. AAPG Bull. 92 (1), 87–125.

Ross, D.J.K., Bustin, R.M., 2009. The importance of shale composition and pore structure upon gas storage potential of shale gas reservoirs. Mar. Pet. Geol. 26, 916–927.

Rouquerol, J., Avnir, D., Fairbridge, C.W., Everett, D.H., Haynes, J.H., Pernicone, N., Ramsay, J.D.F., Sing, K.S.W., Unger, K., 1994. Physical chemistry division commission on colloid and surface chemistry, subcommittee on characterization of porous solids: recommendations for the characterization of porous solids. Int. Union Pure Appl. Chem. 68, 1739–1758.

Schieber, J., 2011. Shale microfabrics and pore development — an overview with emphasis on the importance of depositional processes. Recovery. CSPG CSEG CWLS Convention, pp. 1–4.

Sing, K.S.W., Everett, D.H., Haul, R.A.W., Moscou, L., Pierotti, R.A., Rouquerol, J., Siemieniewska, T., 1985. Reporting physisorption data for gas/sold systems with special reference to the determination of surface area and porosity. Pure Appl. Chem. 57, 603–619.

Slatt, R.M., O'Brien, N., 2011. Pore types in the Barnett and Woodford gas shale: contribution to understanding gas storage and migration pathways in fine-grained rocks. AAPG Bull. 95 (12), 2017–2030.

Stach, E., 1982. Stach's Textbook of Coal Petrology. pp. 295–312 (Berlin. Stuttgart).

Strapoc, D., Mastalerz, M., Schimmelmann, A., Drobniak, A., Hasenmueller, N.R., 2010. Geochemical constraints on the origin and volume of gas of the New Albany Shale (Devonian–Mississippian) in the eastern part of the Illinois Basin. AAPG Bull. 94 (11), 1713–1740.

Tian, H., Pan, L., Xiao, X.M., Wilkins, R.W.T., Meng, Z.P., Huang, B.J., 2013. A preliminary study on the pore characterization of Lower Silurian black shales in the Chuandong Thrust Fold Belt, southwestern China using low pressure N_2 adsorption and FE-SEM methods. Mar. Pet. Geol. 48, 8–19.

Wang, S.Q., Chen, G.S., Dong, D.Z., Yang, G., Lu, Z.G., Xu, Y.H., Huang, Y.B., 2009. Accumulation conditions and exploitation prospect of shale gas in the Lower Paleozoic Sichuan basin. Nat. Gas Ind. 29 (5), 51–58 (in Chinese with English abstract).

Wang, F.Y., Guan, J., Feng, W.P., Bao, L.Y., 2013a. Evolution of overmature marine shale porosity and implication to the free gas volume. Pet. Explor. Dev. 40 (6), 819–824.

Wang, S.B., Song, Z.G., Cao, T.T., Song, X., 2013b. The methane sorption capacity of Paleozoic shales from the Sichuan Basin, China. Mar. Pet. Geol. 44, 112–119.

Wu, J.W., Li, D.P., 2001. Sequence stratigraphic studies of Permian, Wannan area. J. Stratigr. 25, 18–23 (in Chinese with English abstract).

Wu, G.Y., Chen, H.J., Ma, L., Xu, K.D., 2002. Su-Wan block: an independent tectonic unit during period of Tethyan evolution. J. Palaeogeogr. 4 (2), 77–87 (in Chinese with English abstract).

Wu, H., Yao, S.P., Jiao, K., Hu, W.X., Yin, H.W., Jia, D., 2013. Shale-gas exploration prospect of Longtan Formation in the Lower Yangtze area of China. J. China Coal Soc. 38 (5), 870–876 (in Chinese with English abstract).

Xu, M., 2013. Study on Shale Gas of Lower Permian Longtan Formation in Xiangdongnan Depression (Master Dissertation of Chengdu University of Technology. (in Chinese with English abstract)).

Xu, X., Yang, F.L., Zhao, W.F., 2011. Analysis of characteristics of upper hydrocarbon play of Mesozoic–Paleozoic marine group, Lower Yangtze region. Offshore Oil 31 (4), 48–53 (in Chinese with English abstract).

Yu, K., Guo, N.F., 2001. Evaluation on the geology conditions of the Lower Paleozoic hydrocarbon in Lower Yangtze area. Pet. Geol. Exp. 23, 41–46 (in Chinese with English abstract).

Yuan, Y.S., Guo, T.L., Fu, X.Y., Lu, Q.Z., Hu, S.B., 2006. Thermal history and secondary hydrocarbon generation intensity of marine source rocks in Lower Yangtze Area. Geoscience 20 (2), 283–290 (in Chinese with English abstract).

Zhang, H., Zhou, L.Q., Li, J.Q., 2006. Hydrocarbon exploration potential analysis of the Lower Marine Formation assemblage in the Lower Yangtze region. Pet. Geol. Exp. 28 (1), 15–20 (in Chinese with English abstract).

Zhang, J.C., Nie, H.K., Xu, B., Jiang, S.L., Zhang, P.X., Wang, Z.Y., 2008. Geological condition of shale gas accumulation in Sichuan Basin. Nat. Gas Ind. 28, 151–156 (in Chinese with English abstract).

Zhang, J.P., Tang, S.H., Guo, D.X., 2011. Shale gas favorable area prediction of the Qiongzhusi Formation and Longmaxi Formation of Lower Palaeozoic in Sichuan Basin, China. Geol. Bull. China 30, 357–363 (in Chinese with English abstract).

Zhang, D.W., Li, Y.X., Zhang, J.C., Qiao, D.W., Jiang, W.L., Zhang, J.F., 2012a. National Survey and Assessment of Shale Gas Resource Potentials. Geology Publishing House, Beijing (in Chinese).

Zhang, T.W., Ellis, G.S., Ruppel, S.C., Milliken, K., Yang, R.S., 2012b. Effect of organic-matter type and thermal maturity on methane adsorption in shale-gas systems. Org. Geochem. 47, 120–131.

Zhou, D.S., Xu, L.F., Pan, J.P., Huang, X.W., 2012. Exploration prospects of Upper Permian Longtan Formation in Yangtze Block. Nat. Gas Ind. 32, 6–10 (in Chinese with English abstract).

Zhou, Q., Tian, H., Chen, G.H., Xu, Q., 2013. Geological model of dissolved gas in pore water of gas shale and its controlling factors. J. China Coal Soc. 38 (5), 800–805 (in Chinese with English abstract).

Zou, C.N., Dong, D.Z., Wang, S.J., Li, J.Z., Li, X.J., Wang, Y.M., Li, D.H., Cheng, K.M., 2010. Geological characteristics, formation mechanism and resource potential of shale gas in China. Pet. Explor. Dev. 37 (6), 641–653 (in Chinese with English abstract).